Optics & Laser Technology 67 (2015) 86–92

Contents lists available at ScienceDirect

Optics & Laser Technology

journal homepage: www.elsevier.com/locate/optlastec

Methods of resolution enhancement of laser diameter measuring instruments

Yury A. Chursin *, Evgeny M. Fedorov

National Research Tomsk Polytechnic University, 30, Lenin Ave., 634050 Tomsk, Russia

ARTICLE INFO

Article history:
Received 30 May 2014
Received in revised form
11 September 2014
Accepted 29 September 2014

Keywords:
In-process diameter measurement
Diffraction
Spectral analysis

ABSTRACT

The paper presents the implementation of diffraction and spectral analysis methods allowing 1 μm resolution enhancement of optical instruments intended for measurements of such round wire materials as cables, wires, cords, etc. with diameters exceeding the wavelength (~0.5 mm and large). The transformation function suggested allows detecting geometrical boundaries of object's shadows that are used to calculate its diameter independently from its location in the gaging zone. The real-time detection algorithm is described for diffraction extreme values in the analog video signal produced by the charge-coupled device sensors. A method of additional improvement of resolution is shown on the basis of spectral analysis.

1. Introduction

A range of advantages in relation to other optical measuring methods is achieved when the diameter of round wire materials is measured with the help of the laser beam divergence technique [1,2]. Particularly, the lack of catadioptric optical system and movable optical components essentially simplifies the optical system and design of a primary measuring transducer. Design and production of two-dimensional diameter measuring instruments based on this method, is a promising trend in cable instrument engineering due to their reliability, relative ease of fabrication, and objective adjustment.

The laser beam divergence technique for diameter measurement used for long wire materials is based on detection of shadow boundaries of the object by means of multielement linear photodetectors placed in two orthogonal measuring channels. Fig. 1 shows a schematic layout of the optical two-dimensional primary measuring transducer which implements this measurement technique. Traces of laser beams emitted by point radiation sources LAZ_1 and LAZ_2 are shown by dashed lines. These laser beams are directed tangentially to the work piece edges and form light–shadow boundaries t_1f, $t1s$ и t_2f, t_2s on the respective multielement photodetectors CCD_1 and CCD_2. This technique and functions of primary measuring data transformation are described in detail in works [3] and [4].

In practical application, an accurate detection of geometrical boundaries of rising and falling edges of a work piece shadows using a multielement photodetector is rather complicated. This is because the slew rate and the shape of boundaries depend on a local lighting of photodetector and a position of the work piece in a plane orthogonal to the photodetector surface. Scratches, dust, dirt and other during-operation defects of optical glass of measuring instruments affect the accuracy of shadow boundary determination. Even though these defects will be taken into account or effectively eliminated, the accuracy of optical instruments is restricted by diffraction effects occurring at the work piece boundaries that results in a blurring effect of a shadow.

In the patent [5], the principle of the shadow boundary determination is described on the basis of the extreme value distribution from the edge of the opaque object. It is a well-known technique that was investigated in the works [6] and [7]. The principle of the shadow boundary determination is widely used in science and technology [8–16]. In particular, it is applied to enhance the accuracy of geometry measurements of various wire materials. In order to improve a resolution of optical transducers based on a laser beam divergence measurement technique, the analysis of the Fresnel diffraction pattern of large-scale objects was carried out by instruments produced by Sikora and Zumbach Companies. However, in the above mentioned literature, the transformation function allowing the accurate mathematical calculation of the boundary position in measuring wire materials with diameters exceeding the wavelength is not described. This fact restricts the application of Fresnel diffraction by optical transducers based on this technique. In addition to the transformation function, the authors present research into the object movements within the gaging zone affecting the diffraction pattern

* Corresponding author. Postal address: 20,Uchebnaya Str., Apt. 42, 634034, Tomsk, Russia. Tel.: +7 9138684810.
E-mail addresses: _ju_@tpu.ru (Y.A. Chursin), evgeny_fyodorov@list.ru (E.M. Fedorov).

http://dx.doi.org/10.1016/j.optlastec.2014.09.017
0030-3992/

that is very important for the industrial development of measuring devices.

2. Boundary detection method

As shown in Fig. 2, the principle of Fresnel diffraction occurs on the boundary of opaque cylindrical objects. Partially the light penetrates into the shadow region while in the illuminated region it forms the system of diffraction minima and maxima, the difference between them monotonically decreases, and the intensity of light goes to the initial illumination I_0. The distance L between the point source and the multielement photodetector depends on the structural properties of the optical transducer and is constant. The distance y may vary depending on the position of the work piece under control.

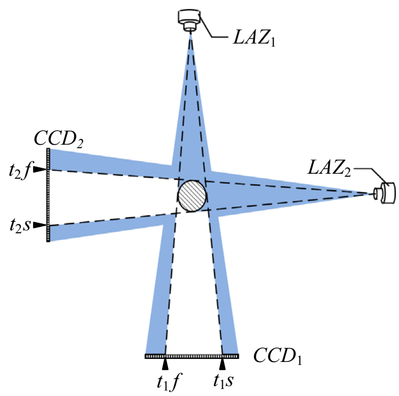

Fig. 1. Laser beam divergence technique for diameter measurement; LAZ_1 and LAZ_2 are point radiation sources; CCD_1 and CCD_2 are multielement photodetectors for the 1st and the 2nd measuring channels, respectively; the quantities t_1f, t_1s and t_2f, t_2s are the shadow boundaries of a work piece under evaluation.

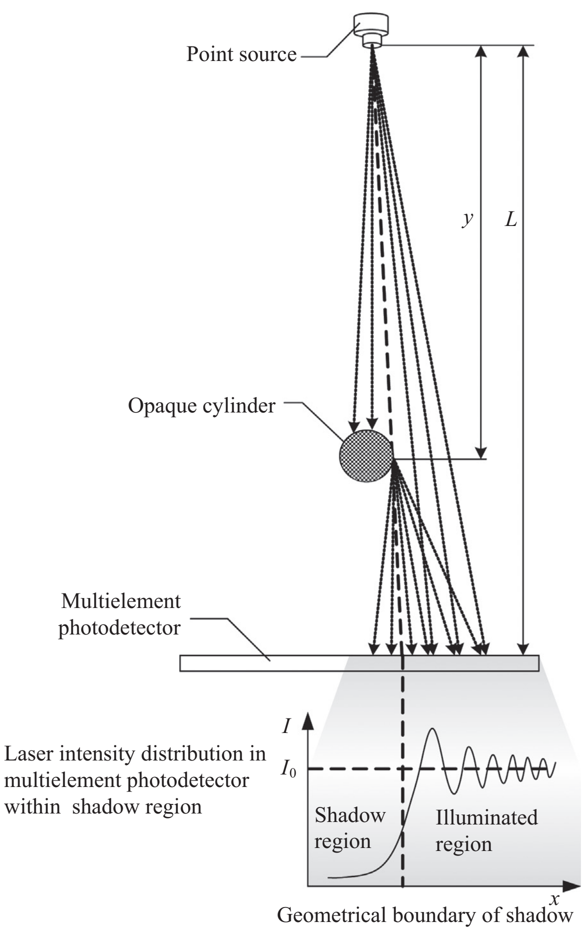

Fig. 2. Fresnel diffraction at the boundary of opaque cylinder: I_0 is the initial illumination; L is the distance between the point source and the multielement photodetector; y is the distance between the point source and opaque cylinder.

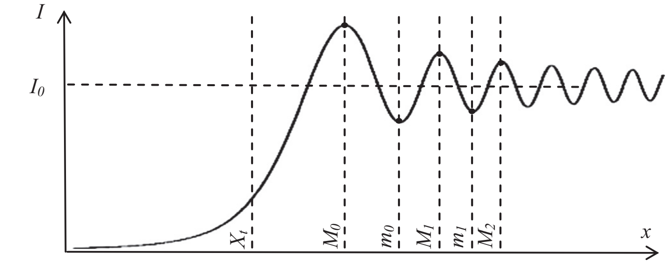

Fig. 3. Diffraction extremum distribution in the vicinity of geometrical boundary: X_t is the geometrical boundary of shadow; M_0, M_1, M_2 are the minima of the first, second and third orders, respectively; m_0, m_1 are the minima of the first and second orders, respectively.

Fig. 3 allows the study of diffraction extremum distribution in the vicinity of geometrical boundary. In case the shadow boundary is projected orthogonally to the photodetector plane, the distance X_i from the point X_t to its respective maximum M_i and the distance x_i from the same point X_t to its respective minimum m_i are defined by formulas

$$X_i = \sqrt{\frac{\lambda L(L-y)}{2y}\left(4i+\frac{3}{2}\right)},\; x_i = \sqrt{\frac{\lambda L(L-y)}{2y}\left(4i+\frac{7}{2}\right)}, \tag{1}$$

where i is the number of the respective maximum or minimum starting from zero; λ is the wavelength of the point source (Fig. 3).

A position of the boundary X_t on the multielement photodetector is the original value for the calculation of diameter using method presented in [3]. Having determined the distance between the first two maxima (interval M_0M_1) or minima (interval m_0m_1) shown in Fig. 3, the boundary X_t can be found. Since factor $\sqrt{\lambda L(L-y)/2y}$ in Eq. (1) is fixed for all extreme values, distribution of these values will then be defined by factors $\sqrt{4i+3/2}$ and $\sqrt{4i+7/2}$ for maxima and minima, respectively. Thus, the distance between the extreme values can change proportionally depending on parameters of L and y, however, correlation between them is being constant. In particular, the interval X_tM_0 correlates with the interval M_0M_1 with fixed coefficient 1.093, while a correlation between intervals X_tm_0 and m_0m_1 equals 2.154. Thus, the formulas below can be derived to find coordinates of geometrical boundaries of rising and falling edges:

$$\begin{aligned} X_{ft} &= 1.093(M_0-M_1)+M_0 = 2.154(m_0-m_1)+m_0 \\ X_{st} &= M_0-1.093(M_1-M_0) = m_0-2.154(m_1-m_0), \end{aligned} \tag{2}$$

where X_{ft} and X_{st} are positions of geometrical boundaries of rising and falling edges; M_0, M_1, m_0, m_1 are the extreme values of diffraction distribution.

3. Experimental

3.1. Measurement setup

The test installation was designed to conduct the experiment. The block diagram of the test installation is shown in Fig. 4, and its implementation in Fig. 5.

The angle measurement was provided by the mechanical dial with 1′ angle-error detection. In the centre of the mechanical dial a board with the multielement photodetector was fixed. The cylindrical object ~4 mm diameter was also mounted in the centre next to the board. The linear CCD (charge-coupled device) NEC μPD8871 was used as a multielement photodetector. It has 3 rows of 10,680 pixels and 4 μm × 4 μm photocell size. CCD scanning rate and exposure time were 1 kHz and about 50 ms, respectively. Diode laser HLDH-808-B20001 with parameters of 808 nm wavelength, 0.2 W optical power, and 42° beam divergence angle, was fixed on a hanger mounted to the dial. A driving pulse generation for the board with the multielement photodetector and laser emitter was performed by the Terasic DE0 Board based on FPGA Cyclone III. FPGA Cyclone III is used to accurately CCD clock and control with 20 MHz frequency observing all intervals in compliance with its datasheet.

Extremum positions for the diffraction pattern were registered by LeCroy WaveSurfer 64Xs Digital Oscilloscope. The test installation was supplied from the power source.

3.2. Experimental results

3.2.1. Estimation of relationships obtained

Fig. 6 shows the oscillogram of the work piece scanned by a laser beam. All the notations used in this figure are taken from Fig. 3.

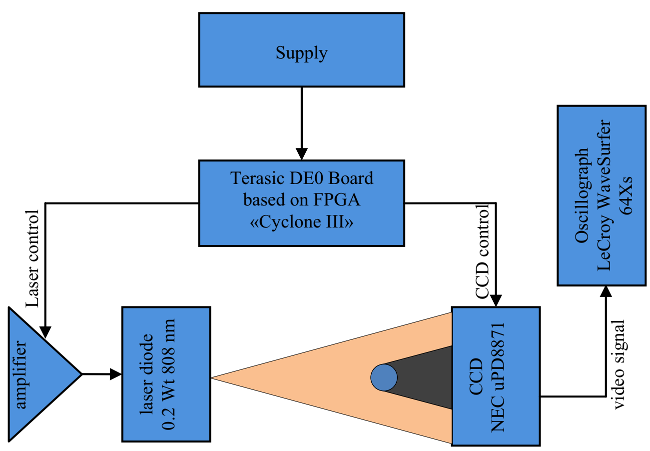

Fig. 4. Block diagram of the test installation.

Fig. 7 shows the experimental dependence between coefficients k_M and k_m (experimentally equal to 2 and 1.1, respectively) and the work piece movement within the gaging zone normal to the multielement photodetector. As shown in Fig. 6, their values are found to be in good agreement with theoretical results. These values are constant within the wide range of the work piece movements that is true for Eq. (2) in case when the diffraction pattern is formed by an incident rim ray normal to the surface of multielement photodetector.

However, in real instruments a work piece can move not only along the axis normal to the photodetector plane but also in any other direction. This results in the fact that rim rays incident at an angle α different from 90°, and the geometry of the optical system including parameters L and y, is transformed to parameters L' and y'. Diffraction extremum distributionis also transformed from X_t, M_i, m_i to $X_{t'}$, $M_{i'}$, $m_{i'}$ states depending on the incident angle α, where X is the geometrical boundary of shadow; M and m are maxima and minima of the i-th order as shown in Fig. 8.

To validate Eq. (2) in case of oblique incidence of rim rays, it is necessary to clarify the manner in which distances between the principle extreme values of the diffraction pattern correlate depending on the angle of incidence. Distances between the first and the second order and between the second and the third order maxima of diffraction pattern were taken as test distances that correspond to intervals M_0M_1 and M_1M_2 shown in Fig. 3.

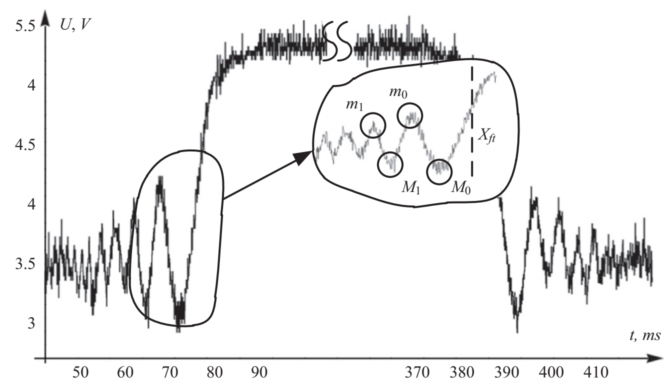

Fig. 6. Oscillogram of the work piece with diffraction effects occurred at the boundaries.

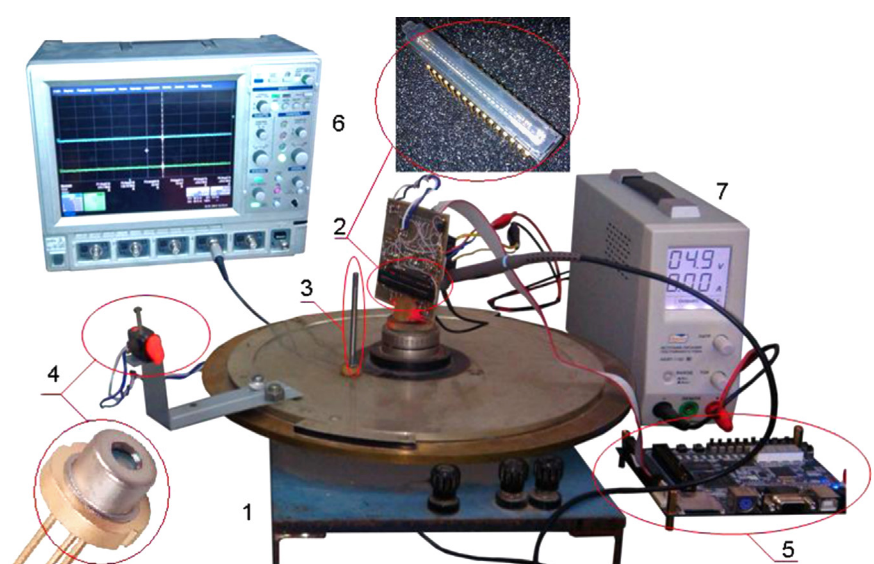

Fig. 5. Test installation: 1—mechanical dial; 2—multielement photodetector; 3—cylindrical object; 4—diode laser; 5—Terasic DE0 Board; 6—LeCroy WaveSurfer 64Xs Digital Oscilloscope; 7—power source.

Diagrams shown in Fig. 9a, demonstrates the empirical relation between intervals M_0M_1 and M_1M_2 and the incident angle α. Zero corresponds to a normal incidence of a rim ray. As it was assumed, distances between the extreme values increase with the increase of beam deflection from the normal to the photodetector plane. As shown in Fig. 9b, the dependence diagram determines a proportionality of a distance change between these extreme values. This diagram demonstrates how the coefficient $k(\alpha)$affects the correlation of M_0M_1/M_1M_2 depending on the angle of incidence. Fig. 9b shows that coefficient $k(\alpha)$ (experimentally equal to 1.35) keeps constant under a wide range of incident angle that proves a proportional change of distances between the extreme values of diffraction pattern. This allows Eq. (2) to be used for an accurate detection of the geometrical boundary of the work piece shadow in a wide range of its movements.

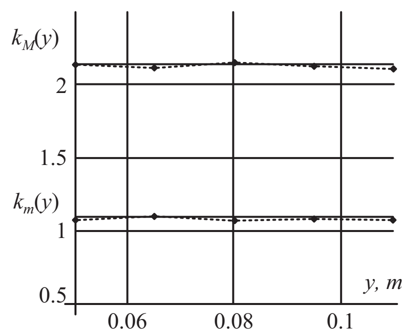

Fig. 7. Dependence between scale coefficients of diffraction and the work piece movements within the gaging zone: $k_M(y)$ and $k_m(y)$ are the coefficients for the first two maxima, respectively.

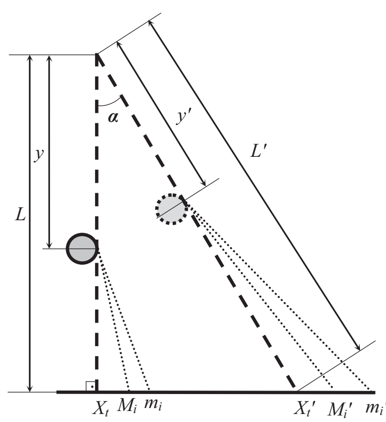

Fig. 8. Formation of diffraction pattern on the multielement photodetector at the angle of incidence α.

3.2.2. Measuring method for geometrical boundary

Thus, the main problem of a preliminary digital signal processing is the calculation of minima (m_1, m_2) and maxima (M_1, M_2) of rising and falling edges so as to further calculate the real boundary of shadow (X_{ft} or X_{st}). To solve this problem, an algorithm shown in Fig. 10 is designed to implement on a field programmable logic device (FPLD).

The derivative sign change detector 1 receives serial data on voltage in CCD cells and clock pulses for cell counts. When the derivative signs changes, the detector transmits a control signal to FIFO buffers 4 and 5. FIFO buffers receive a cell number and a control signal from the derivative sign change detector 1, and then output the latter four cell numbers received. The rising edge detector 2 receives serial data on CCD cell voltage and transmits a control signal to the latch 7 in detecting the rising edge. The falling edge detector 3 receives serial data on CCD cell voltage and transmits a control signal to the cell counter 6 in detecting the falling edge. Cell counter 6 receives a control signal from the

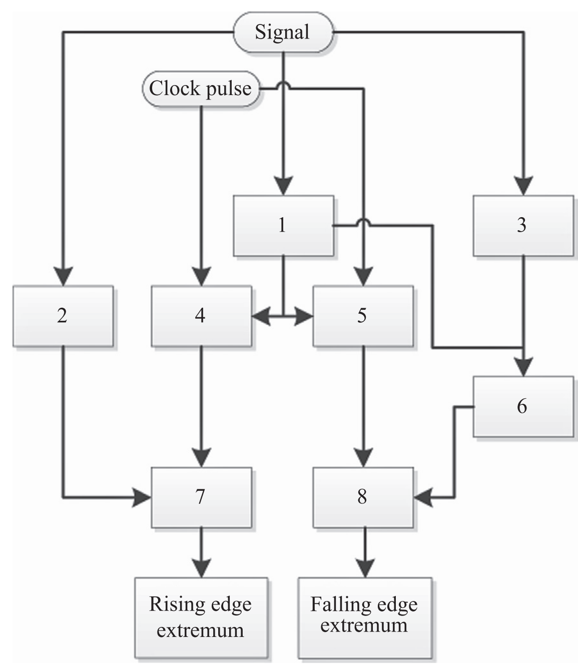

Fig. 10. Algorithm scheme for detecting minima of rising and falling edges: 1—derivative sign change detector; 2—rising edge detector; 3—falling edge detector; 4, 5—FIFO buffers; 6—cell counter; 7, 8—latches.

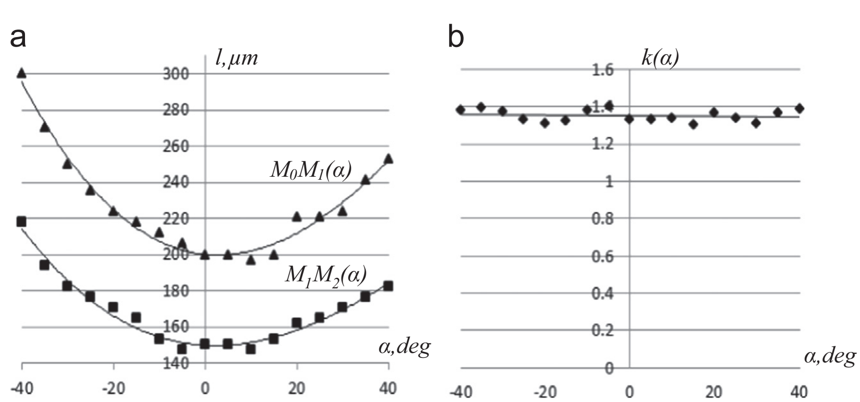

Fig. 9. Diffraction extreme values depending on the rim ray angle of incidence: *a*) M_0M_1 and M_1M_2 relation depending on the angle of incidence α; *b*) coefficient k and incident angle α dependence.

derivative sign change detector 1 and increments internal register's value starting from zero at each change of a signal. Once the internal register achieves value 4, the cell counter will transmit a control signal to latches 7 and 8 from FIFO buffers 4 and 5, respectively. These latches receive four cell numbers each. Register and state reset (except for latches) are carried out upon achieving the upper value of the cell counter or by a start-of-frame signal.

Operating results of the detector are shown in Fig. 11. This figure shows a backward time shift of the detector output so as to illustrate a consistency of extremum determination. Data obtained assist in determination of real positions of geometrical boundaries X_{ft} and X_{st} which are then loaded to microprocessor for processing.

3.2.3. Diameter adjustment using spectral analysis

In constructive proposals of the suggested method of diameter measurement the CCD signal pickup takes about 1 ms. This time interval is defined by CCD maximum clock frequency. Theoretically,

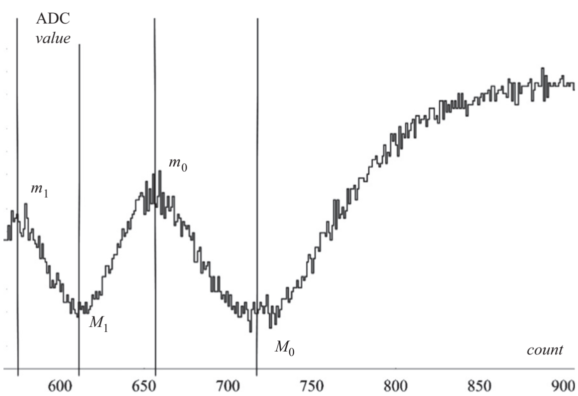

Fig. 11. Detector operating results.

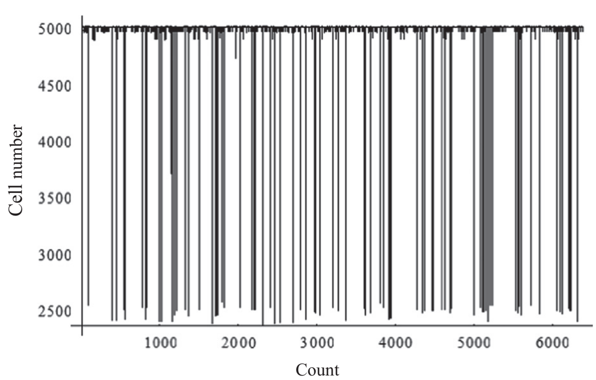

Fig. 12. Initial data sampling for one of the shadow boundaries.

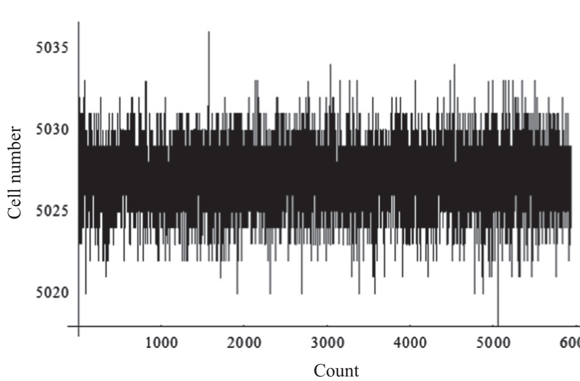

Fig. 13. Data sampling for one of the shadow boundaries after neglecting misses.

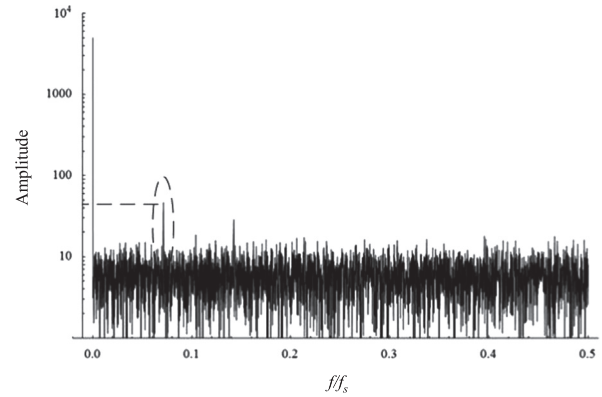

Fig. 14. Data sampling for one of the shadow boundary spectrum.

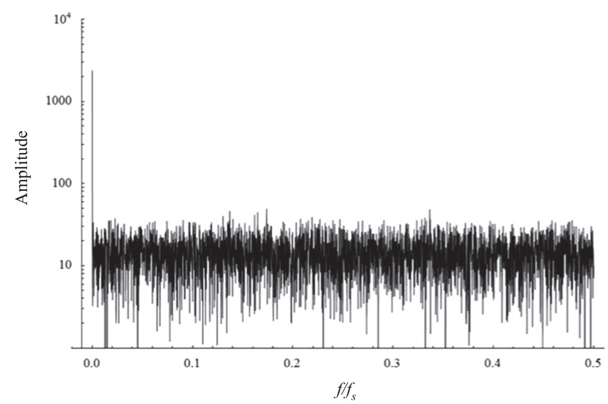

Fig. 15. Spectrum of difference between rising and falling edges.

Table 1.
Rising and falling edges detection error dependently on laser brightness variation using a standard amplitude and the suggested diffraction detector.

I	Amplitude detector		Diffraction detector	
	Rising and falling edges (pixel)	Detection error (μm)	Rising and falling edges (pixel)	Detection error (μm)
$0.95 \cdot I_0$	1875.2	−10.4	1876.7	−0.4
I_0	1877.8	0	1876.8	0
$1.05 \cdot I_0$	1880.7	+11.6	1877.0	+0.8

a work piece can move in the gaging zone due to its vibrations during this interval, and an additional gaging error may occur. However, it can be corrected using a frequency analysis method.

The suggested measuring instrument produces up to 500 frames per second ($f_s = 500$ Hz) for each measuring channel allowing registering oscillation frequency up to 250 Hz.

Let us consider a mechanism of this correction using Figs. 12–15. Fig. 12 contains data sampling for shadow boundaries. It is obvious that these data are incorrect, therefore misses were preliminary neglected as shown in Fig. 13.

The signal is then transformed into the Fourier series. A direct Fourier transform can be written as

$$X_k = \sum_{n=0}^{N-1} x_n e^{-\frac{2\pi i}{N}kn}. \tag{3}$$

At the same time, the oscillation amplitude at frequency $f = \frac{f_s}{2}\frac{k}{N}$ equals to $2|Xk|/N$, $k = 0 \ldots N$ [17].

A spectrum of measured values is shown in Fig. 14. In addition to a constant component this spectrum includes oscillations at 35 Hz

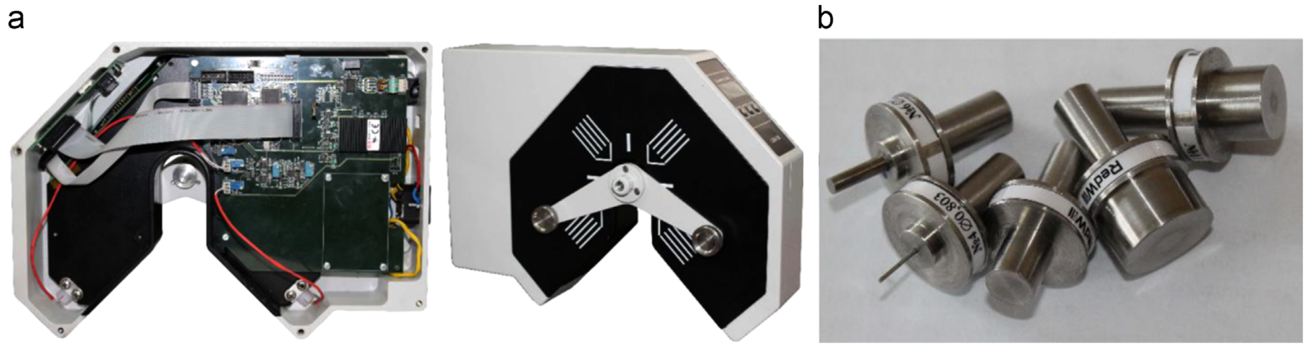

Fig. 16. Instrument prototype and wire gauges. a) Industrial measuring instrument prototype. b) Wire gauges.

frequency. This is either because of vibrations of the work piece occurred within the gaging zone or periodic change of its diameter.

Let us consider the spectrum of difference between rising and falling edges to study the origins of these oscillations (Fig. 15).

Since this spectrum has no large-amplitude oscillations except for their constant component it follows that non-zero oscillations occurred within the rising and falling edges are induced by vibration. With knowledge of the amplitude and frequency of this vibration and CCD scanning rate, it is possible to correct the diameter:

$$dD = t_s V_v = (D/f_{cl})(Af), \tag{4}$$

where t_s is the diameter scanning time; V_v is the linear velocity of the work piece; D is the measured diameter in CCD cells; f_{cl} is CCD clock frequency; A and f are amplitude and frequency of maximum and non-zero oscillations respectively. dD is subtracted from the calculated diameter since vibration affects the accuracy of diameter measurement.

3.3. Discussion

Techniques suggested in this work were tested at various intensities of laser radiation similar to a real operation of a measuring instrument. Results of investigation are shown in Table 1 as compared to those obtained for a classical amplitude detector which detects shadow position by the slew rate and the shape of boundaries on the CCD picture.

The detection error for the shadow boundary as shown in Fig. 6, comes to 10 μm at laser brightness variation $\pm 5\%$ from a certain initial value I_0. During operation, this error can increase multiple times due to contamination of optical elements, detection errors of rising and falling edges being summed up for the diameter calculation. In suggested technique of the boundary detection (by diffraction pattern extreme values) the error is around 1 μm at the similar flare brightness. This provides high metrological characteristics of measuring instruments regardless of the optic emitter drift characteristics and purity of optics instruments.

Suggested techniques were approved on many opaque cylindrical objects with diameters ranging from 0.5 to 40 mm and made of different materials such as polypropylene, polyethylene, polyvinylchloride, rubber, metals, etc. Semiconductor diodes 808 nm length and 0.2–0.5 W energy were used in this study. As a rule, they possess different beam divergence along different symmetry planes, in particular $\Theta// \approx 8 \div 11^\circ$, $\Theta\perp \approx 39 \div 48^\circ$. In the laser beam divergence technique for diameter measurement, only semiplane $\Theta\perp$ is used to provide a flare of the entire gaging zone. Therefore, other laser positions and, consequently, differences in the light beam polarization are not presented in this paper.

Depending on a configuration of the optical system, suggested techniques provide resolution for a single diameter measurement within 2–3 μm range allowing for optical magnification of a laser-beam-divergence optical transducer (Fig. 1). Further mathematical processing of obtained data in conformance with methodology described in works [3,4] as well as the dataset statistical analysis allows obtaining the general resolution up to 1 μm and lower for the optical system.

Estimation of feasibility of the suggested techniques was carried out with the industrial measuring instrument prototype which was designed by the authors (Fig. 16a). Wire gages (from 0.5 to 20 mm) certified at the State Metrological Agency with accuracy of 0.5 μm have been used (Fig. 15b). Dimensions of this prototype are 240 mm length; 175 mm height; 57 mm width. Maximum diameter to be measured is 20 mm.

Accuracy of measurement comes to 1 μm. Harmonic interference with frequency up to 250 Hz are eliminated. Scanning rate achieves 1 kHz for each measuring channel. It should be noted that object to be measured include such wire materials as cables, cords, polymer tubes, and other products obtained by the extruding technique. The roughness of their surface achieves, as a rule, several dozens and hundreds micrometers, therefore they cannot be referred to a class of polished or reflective surfaces. In measuring cylindrical objects having a high specular reflection factor, effects described in works [18,19] should be taken into account.

4. Conclusions

The paper investigates a method of measurement of various kinds of round work piece diameters allowing to accurately resolute the diffraction pattern and detect positions of extreme values to calculate positions of geometrical shadow boundaries. A formula was obtained to accurately determine geometrical position of the work piece shadow without analyzing rising and falling edges of a work piece shadows. Algorithm of physical implementation of the given method in electronic computers was suggested. A frequency analysis algorithm was suggested for additional correction of diameter measurement. Application of the suggested methods and algorithms together with the conversion function described in works [3,4] allows designing instruments for measuring the diameter by laser in non-contact way with high accuracy.

Acknowledgments

The authors gratefully acknowledge the great assistance of A. Itiligator from Tomsk Polytechnic University and translation by M. Vorob'eva from Tomsk State University of Architecture and Building.

References

[1] Tay CJ, Toh SL, Shang HM. Time delay and integration imaging for internal profile inspection. Opt Laser Technol 1998;30(8):459–65 (November).

[2] Jinhui Lan Jian Li, Hu Guangda, Zeng Yiliang. Distance estimation using a panoramic sensor based on a novel spherical optical flow algorithm. Opt Laser Technol 2013;45:168–76 (February).

[3] Svendrovskii A.R., Raschet diametra v beskontaktnykh dvukhkoordinatnykh izmeritelyakh [Measurement of diameter by non-contact two-dimensional detectors]. In: Proceedings of the . 1st all-Rusian. science. conference on ‘Scientific and Engineering problems of instrument engineering. Tomsk; 2005. p. 31–33.

[4] Fedorov E.M., Edlichko A.A. Vychislenie geometricheskikh parametrov dvukh-koordinatnykh izmeritelei diametra protyazhennykh izdelii [Calculation of geometrical parameters of two-dimensional instruments used for measuring diameter of long wire materials]. Bulletin of the Tomsk Polytechnic University, 2008. No. 2. (rus).

[5] Measurement of diameter using diffraction borders and electronic soiling correction, Patent N EP 0924493 B1. Adrian Beining, Werner Dr.-Ing. Blohm, HaraldSikora; 2002.

[6] Sommerfeld A. (German edition 1950, English translation). Optics. New York: Academic Press; 1964 (sec 37, 38).

[7] Born, Wolf E. Principles of Optics. 3rd Edition. Oxford: Pergamon Press; 1965.

[8] Toenshoff HK, Tuennermann A, Korthals J. Use of Fresnel diffraction for the measurement of rotational symmetrical workpieces. Proc SPIE Int Soc Opt Eng 1999;3784:334–43.

[9] Chi-Tang Li James V Tietz. Improved accuracy of the laser diffraction technique for diameter measurement of small fibres. J Mater Sci 1990;25(11):4694–8.

[10] Khodier SA. Measurement of wire diameter by optical diffraction. Opt Laser Technol 2004;36(1):63–7 (Original Research Article).

[11] Durgin GD. The practical behavior of various edge-diffraction formulas. IEEE Antennas Propag Mag 2009;51(3):24–35.

[12] George S. Straight edge diffraction using a laser. Phys Educ 1972;7(6):349–52.

[13] Li Jinhuan, Sasaki Osami, Suzuki Takamasa. Measurement of diameter of metal cylinders using a sinusoidally vibrating interference pattern. Opt Commun 2006;260(2):398–402.

[14] Jabłoński R, Mąkowski J. Measurement of cylinder diameter by laser scanning. Recent Adv Mechatron 2007:596–600.

[15] Chugui Y., Bazin V., Finogenov L., Makarov S., Verkhogliad A. Optical electronic measuring systems and laser technologies for scientific and industrial applications. In: Proceedings of the international symposium on instrumentation and control technology No. 6, Beijing, China. 2006. vol. 6357 (2) [Note(s): 2 vol.] (13 ref.) isbn:0-8194-6452-x; 978-0-8194-6452-1.

[16] Jablonski Ryszard, Pawel Fotowicz. New generation of laser mike. Proc. SPIE 2001 (Laser Metrology for Precision Measurement and Inspection in Industry, 91 (September 11).

[17] Smith SW. Chapter 8: The Discrete Fourier Transform". The Scientist and Engineer's Guide to Digital Signal Processing. Second ed.. San Diego, California: California Technical Publishing; 1999.

[18] Sanchez-Brea Luis Miguel, Martinez-Anton Juan Carlos. Eusebio Bernabeu Effect of the refraction index in the diameter estimation of thin metallic wires. Proc. SPIE 2005;5858:585819. http://dx.doi.org/10.1117/12.612652 (August 26).

[19] Lars Benckert Lars Forsberg, Molin Nils-Erik. Fresnel diffraction of a Gaussian laser beam by polished metal cylinders. Appl Opt 1990;29(3):416–21.